Available online at www.sciencedirect.com
SCIENCE DIRECT
Polymer 46 (2005) 3818–3830
polymer
www.elsevier.com/locate/polymer

# Poly(styrene-*co*-acrylonitrile)/montmorillonite organoclay mixtures: a model system for ABS nanocomposites

H.A. Stretz[a], D.R. Paul[a,*], P.E. Cassidy[b]

[a]*Department of Chemical Engineering and Texas Materials Institute, University of Texas at Austin, Austin, TX 78712, USA*
[b]*Institute for Environmental and Industrial Science, Texas State University-San Marcos, San Marcos, TX 78666-4616, USA*

Received 28 January 2005; accepted 9 March 2005

**Abstract**

Dispersion of clay particles in acrylonitrile–butadiene–styrene (ABS) and styrene–acrylonitrile copolymer (SAN) nanocomposites with montmorillonite (MMT) have been compared to assess whether ABS/MMT nanocomposite behavior can be adequately modeled using the simpler SAN/MMT system. Electron microscopy photomicrographs show that clay particles in ABS/MMT composites reside in the SAN matrix phase and accumulate at the rubber particle surfaces. In mixtures of four organoclays with the two polymers, WAXS (wide angle X-ray scattering) peak height and shift in gallery height was the same for a given organoclay. Aspect ratios determined through image analysis were also the same in each polymer. Modulus enhancement as measured by an exfoliation efficiency index showed the same patterns for each organoclay in the two matrices, but the ABS/MMT composites had consistently lower efficiencies than in SAN/MMT composites. This trend is expected to be due to the variations in orientation of clay particles in ABS/MMT composites at the rubber particle surface. In summary, SAN/MMT composites represent a good model system for ABS/MMT.


*Keywords:* ABS; SAN; Montmorillonite

## 1. Introduction

Halogenated fire retardants (FR) found in acrylonitrile–butadiene–styrene copolymer (ABS) plastic computer housings (e.g. decabromodiphenyl ether), will be limited as recycle content by pending European Union legislation as early as 2006 [1–8]. The alternative inorganic FRs are often incorporated at such high loadings, i.e. up to 50 wt%, that there is a significant compromise in the final balance of properties for the composite, particularly toughness. Formation of a nanocomposite by addition of montmorillonite clay platelets (MMT) to the polymer is another potential approach which has been shown to be effective at low loadings (<5%), and may lead to a better balance of physical properties. For example, nanocomposites of MMT with nylon 6 [9,10] and with polypropylene (plus a PP grafted with maleic anhydride as a compatibilizer) [11–13] have shown substantial improvement in the FR properties (up to 70% reduction in the peak heat release rate) with simultaneous improvements in modulus and strength. There is still some minimal compromise in composite toughness [14,15], and typically the state of disaggregation of the clay platelets, or exfoliation, is considered to be a key factor in developing good composite properties.

The properties of melt-processed ABS/MMT composites have been reported by Hu et al. [16,17]. Masterbatch approaches to improved exfoliation have been investigated by Wilkie et al. and Zhang et al. [18–20], and emulsion as well as in situ polymerization efforts have been reported by Jang et al. [21]. In all cases TEM images showed evidence of incomplete exfoliation in terms of MMT particle thickness as compared to typical particle thicknesses noted in well-exfoliated nylon 6/MMT nanocomposites [14]. With regard to flammability, a recent report by Hu et al. [22], showed a 68% reduction in the peak heat release rate of ABS/MMT composites using a synergistic mixture of antimony–halogen flame retardants and MMT. The magnitude of this reduction suggests that MMT clays do have FR potential in ABS systems. While the halogen content in the aforementioned formulation is greatly reduced from

* Corresponding author. Tel.: +1 512 471 5392; fax: +1 512 471 0542.
*E-mail address:* drp@che.utexas.edu (D.R. Paul).

0032-3861/$ - see front matter © 2005 Elsevier Ltd. All rights reserved.
doi:10.1016/j.polymer.2005.03.043

traditional FR grade ABS, improved exfoliation of the MMT might further reduce or even eliminate the need for the halogen. The authors cited herein were primarily interested in thermal and flammability properties of the ABS/MMT composites, and the contribution of extent of exfoliation to mechanical properties in these mixtures has not yet been fully explored.

This investigation is the second publication in a series examining ABS/MMT nanocomposites and the effect of exfoliation on the balance of properties. In the initial publication we presented the effect of surfactant structure, varied in a systematic manner, on mechanical properties and extent of exfoliation for poly(styrene-*co*-acrylonitrile) (SAN)/MMT nanocomposites [23]. The rationale behind studying such composites was that SAN is the matrix phase of the multiphase ABS; thus SAN/MMT might be considered a model system useful for understanding ABS/MMT compatibility. In the current study we have addressed two issues implicit in this assumption. First, for the simplest case of drop-in addition of ABS and MMT during melt-processing, do the clay particles selectively accumulate in the SAN matrix phase? Second, are the patterns of intercalation, reinforcement and clay morphology similar when comparing composites of MMT with SAN versus ABS?

A select number of surfactant-modified clays have been examined in the present study, using both SAN and ABS as the composite matrix. The ABS grade chosen is used commercially in business machine applications. The composite properties for both mixtures were compared using electron microscopy, wide angle X-ray scattering (WAXS) and Young's modulus. The effect of clay addition on impact and strength properties in the ABS/MMT composites is also discussed.

## 2. Experimental

### 2.1. Materials

The SAN and ABS materials are described in Table 1. A description of the organic ammonium surfactants used to form organoclays from montmorillonite clay materials is given in Table 2. All organoclays were supplied by Southern Clay Products. Four variations in the clay surfactant structure were explored, see Fig. 1. The exchange ratio of the surfactant on the MMT surface was 95 mequiv./100 g clay (MER) for all of the clays. The cation exchange capacity (CEC) of the clay is about 92 MER; thus, there is an approximate stoichiometric exchange of surfactant for native cations of the montmorillonite. The organoclay has 30–40% more mass than the inorganic MMT platelets, and the organic composition is characterized by a loss on ignition (LoI), see values reported in Table 2.

### 2.2. Methods

Melt blended composites were prepared using a Haake co-rotating, intermeshing twin screw extruder (diameter = 30.5 mm, $L/D = 10$) at 280 rpm, a barrel temperature of 220 °C, and a feed rate of 980 g/h. Extruder screw configuration, rpm and feed rates matched those optimized from previous studies of nanocomposite formation using this extruder [24,25]. All materials were dried overnight under vacuum at 80 °C prior to use. The aluminosilicate content (MMT) was determined from ash content ($MMT_{ash}$) of dried pellets at 900 °C for 45 min. The weight percent MMT was then calculated from the ash content by the following equation,

$$\mathrm{MMT} = \frac{\mathrm{MMT_{ash}}}{0.935} \tag{1}$$

The numerical factor corrects for structural rearrangements of the pristine montmorillonite during ash analysis, resulting in a 6.5% mass loss [26]. Further, details regarding calculation of organoclay content have been previously published [14,23,27].

Tensile and Izod bars (ASTM D638 and ASTM D256, respectively) were formed using an Arburg Allrounder 305-210-700 injection molding machine. Test specimens were molded at a barrel temperature of 260 °C, and a mold temperature of 80 °C. Mechanical testing was performed on an Instron model 1137 at a crosshead speed of 0.51 cm/min. To obtain the elongation at break, specimens were tested at 5.1 cm/min. The notched Izod impact test results were

Table 1
Description of matrix materials

| Material | Supplier | Density ($g/cm^3$) | Brabender torque[a] (N m) | Young's modulus (GPa) | Tensile strength (MPa) | Comments |
|---|---|---|---|---|---|---|
| SAN-25 | Dow Tyril® 100 | 1.07 | 11.3 | 3.47 | 71.7 | AN content = 25%; $M_w$ = 152 kg/mol |
| ABS | GE Cycolac® GPM5500 natural | 1.04 | 12.0 | 2.27 | 44.8 | MFR = 7.0 g/10 min<br>Notched Izod Impact = 294 J/m<br>DTUL@66 psi-unannealed (0.64 cm) = 96 °C<br>TEM-based estimate of rubber particle size: ~0.02–0.2 μm |

[a] Values taken at 220 °C and 60 rpm.

Table 2
Description of organoclay materials

| Organoclay[a] | Commercial designation | Quaternary ammonium ion | Percent loss on ignition (LoI) | $d_{001}$ Spacing (WAXS) (nm) |
|---|---|---|---|---|
| $(HE)_2MT$ | 30B | Bishydroxy-ethyl methyl tallow | 30 | 1.78 |
| $BM_2(HT)$ | Experimental | Benzyl dimethyl hydrogenated tallow | 32.1 | 1.86 |
| $(EHex)M_2(HT)$ | 25A | 2-Ethylhexyl dimethyl hydrogenated tallow | 34 | 1.81 |
| $M_2(HT)_2$ | 20A | Dimethyl dihydro-genated tallow | 38 | 2.55 |

[a] T, tallow; HT, hydrogenated tallow; C*, coco; M, methyl; B, benzyl; H, hydrogen; (EHex), 2-ethylhexyl; ($C_{18}$), palm oil derivative; (HE), hydroxyethyl. All clays have 95 MER (mequiv./100 g resin) of surfactant.

measured using a TMI tester at room temperature with a 5 ft·lb hammer.

WAXS scans were obtained using a Sintag XDS 2000 diffractometer through the courtesy of Southern Clay Products using oriented injection molded tensile bars so that the beam probed the skin of the bar perpendicular to the direction of flow.

Samples for electron microscopy were sectioned using a Reichert-Jung Ultracut E cryogenic ultramicrotome to a thickness of about 50–70 nm with the knife at room temperature for SAN samples, and at −45 °C for the ABS samples. Knife speed was 0.5 mm/s. The sections were imaged using a JEOL 2010 F electron microscope operating at 120 kV. In order to improve contrast, some of the images presented here were taken in scanning transmission electron microscopy (STEM) mode using a high angle annular dark field detector (HAADF) [28]. Thus, MMT particles appear white, while the polymer matrix appears black. Grey shades are believed to arise from imperfect orientation of the clay platelet. Samples were also imaged in transmission electron microscopy (TEM) mode, and these have a grey matrix and black montmorillonite particles. Both are presented without further comment as they are easily differentiated. The ABS samples were photographed in both pristine and stained form in order to provide optimized information about the location of the clay platelets, and appropriate notation regarding stained or unstained samples is given in the text. The stained sections were exposed on their grids to $OsO_4$ vapor for 24 h. All specimens were ultramicrotomed such that the reported images represent views along the flow direction (FD).

Image analysis was performed on digitally captured images using 100–200 particles from over four different sites in TEM mode. Gatan Digital Micrograph analysis software was employed to measure the length and thickness of each feature, with manual highlighting of the individual features.

## 3. Morphology

### 3.1. Waxs

The structure of the clay surfactant is well known to affect the shift in the platelet gallery spacing relative to the original organoclay spacing, $\Delta d_{001}$, upon blending with polymer. In the present study, a small group of organoclays with varying surfactant structures were chosen in order to achieve a range of exfoliation levels. These materials and related ones have been previously discussed in connection with SAN/MMT nanocomposites [23].

A summary of the shift in gallery heights ($\Delta d_{001}$) for all of the MMT composites with ABS and SAN is given in Table 3. The composites formed using SAN and ABS all exhibited X-ray peaks characteristic of unexfoliated clay particles. For any given organoclay, the peak locations are consistently the same in SAN and ABS. An example of the WAXS scans for the $M_2(HT)_2$ organoclay in each polymer is shown in Fig. 2. The character of the peaks as well as the magnitude of the $d_{001}$ shift ($\Delta d_{001} = d_{001,\ \text{composite}} - d_{001,\ \text{pristine organoclay}}$) remained unchanged whether the polymer matrix was SAN or ABS. The same effect was observed for all four organoclays. Thus, the ability of these two polymers to swell the clay crystallites is similar if not identical, and the rubber particles in ABS/MMT composites do not appear to affect the swelling process. The order of the shift of $\Delta d_{001}$ for both matrices is:

$$(HE)_2MT > BM_2(HT) > (EHex)M_2(HT) > M_2(HT)_2$$

### 3.2. TEM and STEM photomicrographs

TEM and STEM photomicrographs for composites of

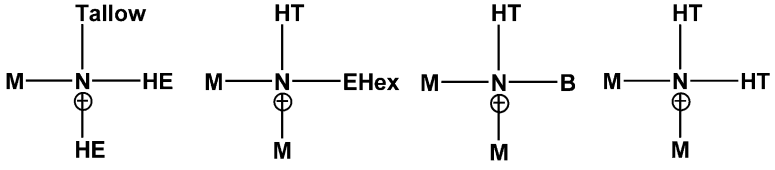


Fig. 1. Structures of quaternary ammonium ions used to form MMT organoclays; T = tallow, HT = hydrogenated tallow, M = methyl, B = benzyl, (EHex) = 2-ethylhexyl, (HE) = hydroxyethyl.

Table 3
Shifts in gallery height for ABS/MMT versus SAN/MMT composites

| Organoclay[a] | $d_{001}$ (nm) | | | $\Delta d$ (nm) | |
|---|---|---|---|---|---|
| | Pristine organoclay | ABS/MMT composites | % MMT | ABS/MMT | SAN/MMT[b] |
| $(H)_2MT$ | 1.78 | 3.22 | 3.0 | 1.44 | 1.48 |
| $BM_2(HT)$ | 1.86 | 2.93 | 3.3 | 1.07 | 1.16 |
| $(EHex)M_2(HT)$ | 1.81 | 2.90 | 2.8 | 1.09 | 1.04 |
| $M_2(HT)_2$ | 2.55 | 3.12 | 3.0 | 0.57 | 0.57 |

[a] T, tallow; HT, hydrogenated tallow; M, methyl; B, benzyl; (EHex), 2-ethylhexyl; (HE), hydroxyethyl.
[b] Information onWAXS scans for the SAN/MMT composites are given in greater detail a previous publication [23].

SAN with two of the organoclays, $(HE)_2MT$ and $M_2(HT)_2$, are shown in Figs. 3 and 4. These photomicrographs illustrate the range of particle morphologies found in the SAN mixtures. There are some differences in the character of the stacks for these two materials. The stacks are thicker for the $(HE)_2MT$ composite and the platelets within the stack appear to be much more twisted and irregular. Number average stack lengths and thicknesses are reported in Table 4 for these two composites, with the data for $(HE)_2MT$ taken from a limited number of photomicrographs which showed primarily regular particles for this composite. Images for $BM_2(HT)$/SAN and $(EHex)M_2(HT)$/SAN composites exhibited similar distortions which complicated quantitative digital image analysis.

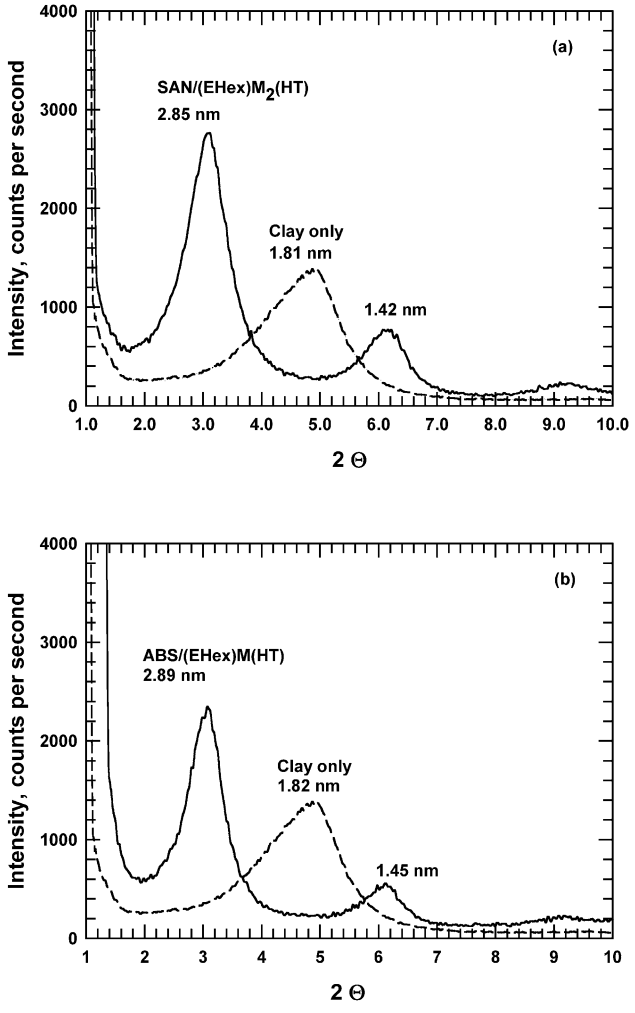


Fig. 2. Comparison of WAXS scans for representative composites and the pristine organoclays including: (a) SAN/$(EHex)M_2(HT)$ at 1.9% MMT versus (b) ABS/$(EHex)M_2(HT)$ at 2.8% MMT.

STEM images for blends of ABS with the organoclays are more complex in that there are now two dispersed phases to consider, the impact modifier (rubber particles), and the filler (MMT). The rubber phase is carbon-based, which is easily detected when stained with a heavy metal oxide ($OsO_4$) to provide visual contrast with the SAN matrix phase. The filler phase is an aluminosilicate and is easily differentiated from the SAN matrix phase by mass contrast without staining. However, when the rubber phase is stained with heavy metals, this causes both clay particles and rubber particles to appear bright in the STEM images, and clay particles in contact with rubber particles cannot be differentiated. Both stained and unstained images of ABS/MMT composites are presented and the combination of these images gives an overall picture of the morphologies of all phases as well as where the clay particles reside with respect to the rubber and matrix phases.

Fig. 5 shows a photomicrograph of the unfilled, stained virgin ABS. The supplier did not provide details of the ABS production or structure, but given the ~0.2 μm size of many of the rubber particles, it is believed that this is an emulsion-made rubber. Fig. 6 shows comparable photomicrographs for the stained ABS/$(HE)_2MT$ composite. Note that the rubber phase appears relatively unaltered for either filled or unfilled ABS. However, in comparing the clay particles in the ABS/$(HE)_2MT$ composite with the clay particles in the

Table 4
TEM image analysis of organoclay particles in selected nanocomposites

| Nanocomposites | Number avg. length $\overline{l_n}$ (nm) | Number avg. thickness $\overline{t_n}$ (nm) | Aspect ratio $\overline{l_n}/\overline{t_n}$ | Number avg. aspect ratio $\langle l/t\rangle_n$ |
|---|---|---|---|---|
| SAN/$(HE)_2MT$ | 184 | 7.6 | 24.2 | 31.6 |
| SAN/$M_2(HT)_2$ | 299 | 8.2 | 36.5 | 48.9 |
| ABS/$(HE)_2MT$ | 120 | 5.9 | 20.3 | 28.2 |

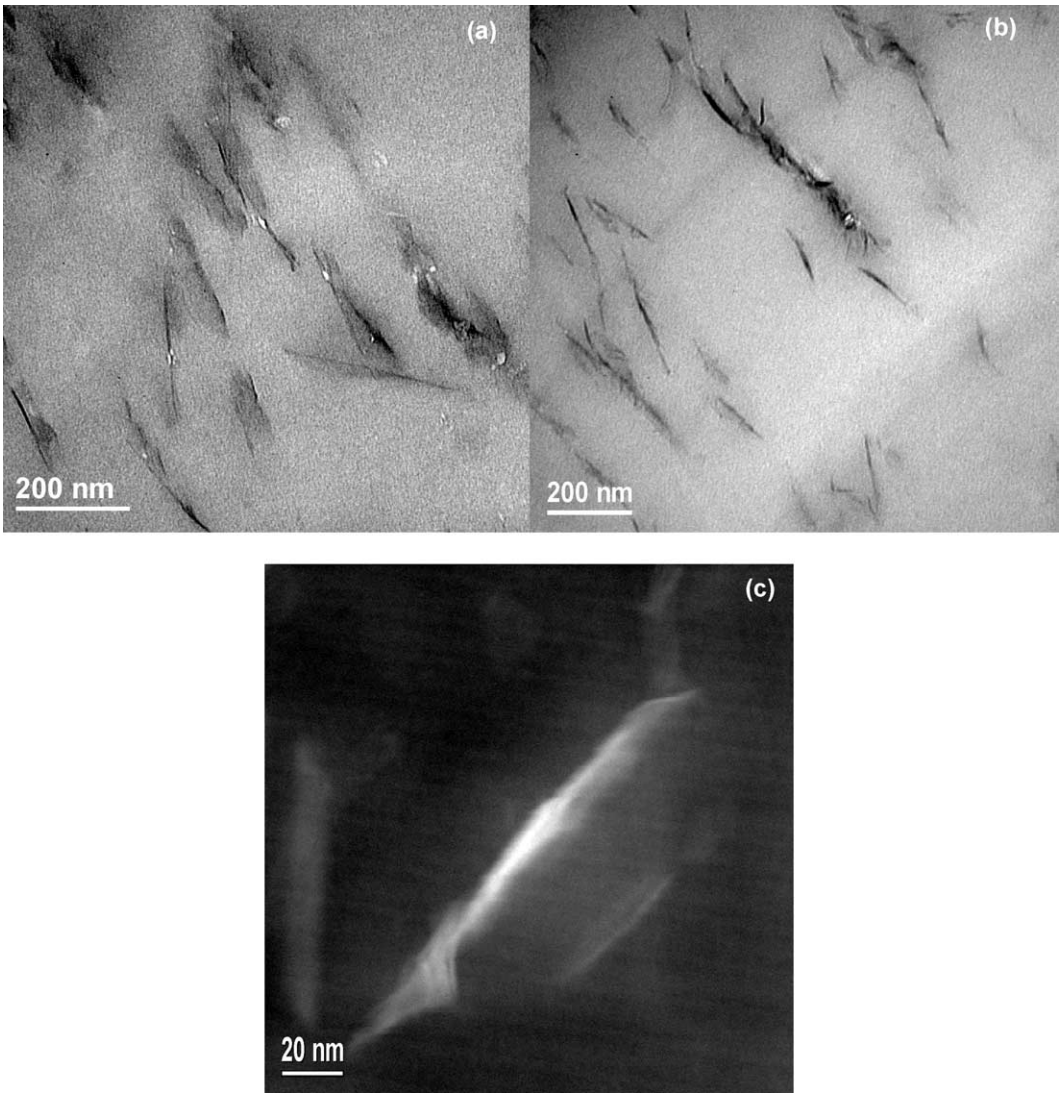


Fig. 3. STEM photomicrographs of SAN/$(HE)_2$MT composite at 1.9% MMT. Note that some of the stacks appear to have twisted/spiral morphologies.

SAN/$(HE)_2$MT composite (Fig. 6 versus Fig. 3, respectively), fewer clay particles per unit area are apparent in the ABS images than in the SAN images, despite similar MMT content. Furthermore, there is a tendency for some ends of the clay particles in the ABS/$(HE)_2$MT composites to be oriented towards a rubber particle. This is most clearly seen in Fig. 6(d), where the rubber particle appears to be distended towards the clay surface.

Fig. 7 shows photomicrographs of the unstained ABS/$(HE)_2$MT composite. The rubber particles are not visible in this image, but the sites they occupy in the SAN matrix are apparent as 'holes'. Several interesting observations can be deduced from this series of images. The clay particles appear to be attracted to and conform to the rubber particle surfaces. This observation may resolve the discrepancy of fewer clay particles per unit area seen in the stained ABS images, since clay particles in contact with stained rubber particles cannot be differentiated easily. Also, higher magnification images shown in Fig. 7 reveal variations in orientation not seen in the SAN/MMT composites, since some of the ABS/MMT clay particles are aligned with the rubber particle surfaces. Finally, note that none of the clay particles were detected inside the crosslinked rubber phase.

In summary, the clay particles in the ABS/MMT nanocomposites reside in the SAN matrix phase with some accumulation at the rubber particle surfaces. There are numerous influences, thermodynamic and kinetic, which could cause the clay particles to reside at the rubber particle surface. Analagous three phase polymer blends and the driving forces behind accumulation at an interface have been discussed by Cheng et al. [29]. Bousmina et al. have reported a similar distribution of phases in PS/PP/MMT composites and provide a thorough review of other polymer/montmorillonite composites in which accumulation of the MMT at the interface between two polymer phases has been observed [30].

Digital image analysis results comparing ABS/$(HE)_2$MT nanocomposite features to those for SAN/MMT are given in

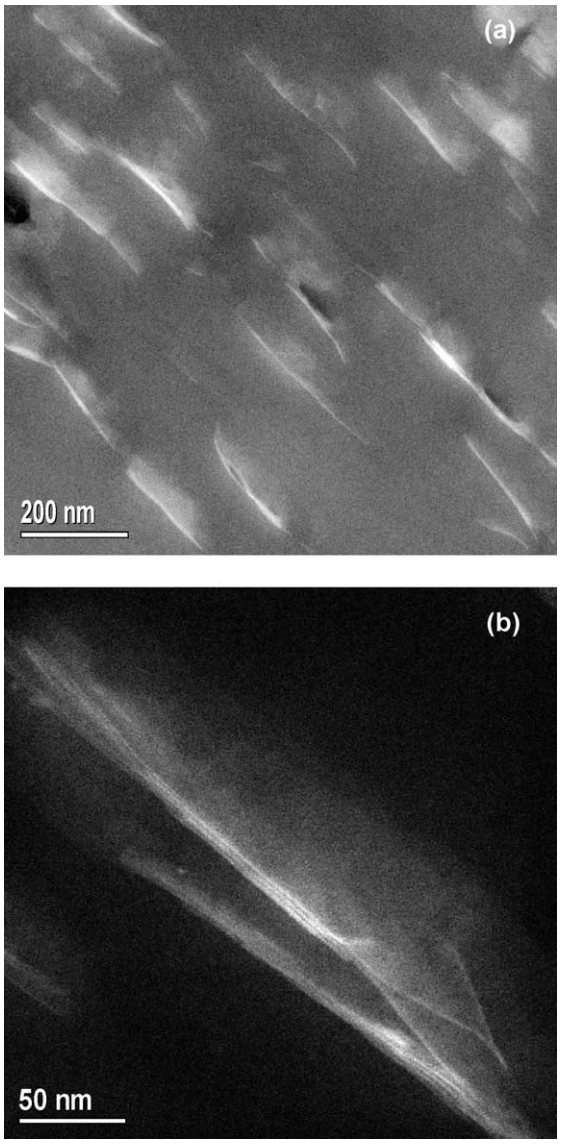


Fig. 4. STEM photomicrographs of SAN/$M_2(HT)_2$ composite at 2.1% MMT.

Table 4. Two different methods for calculating aspect ratio are presented, representing two variations for managing the collected data files. Previous publications from this laboratory reported aspect ratios determined using well-exfoliated nanocomposites [31,32]. The precision of particle thickness measurement was optimized by using a calculation based on both WAXS $d_{001}$-spacing data and visual counts of the number of particles in a stack [31]. The data files for particle lengths and particle thicknesses were, thus, collected separately. The aspect ratios reported were determined as a ratio of the number average length $(\bar{l})_n$ and the number average thickness $(\bar{t})_n$.

$$(\bar{l})_n = \frac{\sum n_i l_i}{n}, \quad (\bar{t})_n = \frac{\sum n_i t_i}{n} \tag{2}$$

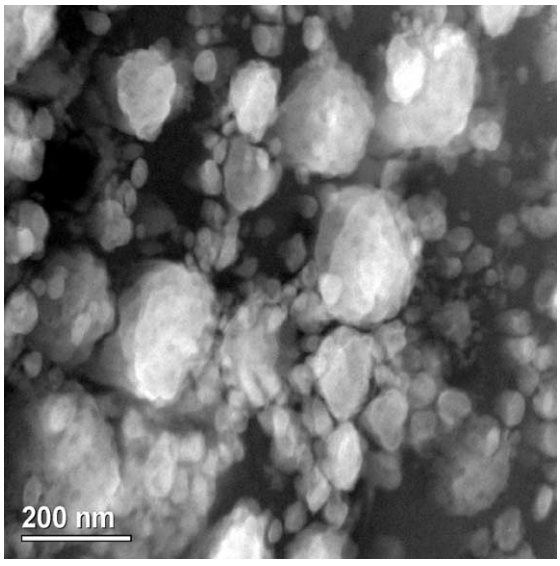


Fig. 5. STEM photomicrograph of ABS, stained; rubber particles appear bright, and SAN matrix is grey.

$$\mathrm{AR} = \frac{(\bar{l})_n}{(\bar{t})_n} \tag{3}$$

Another method for calculating such an average is to collect an additional file of the aspect ratios of the individual particles, and subsequently take the number average of these individual values.

$$\mathrm{AR} = \left\langle \frac{l}{t} \right\rangle_n = \frac{\sum n_i \left(\frac{l}{t}\right)_i}{n} \tag{4}$$

The two calculations give a different view of the distribution of particle thicknesses and lengths.

Referring again to Table 4, while there are variations in the number average length and thickness of the MMT particles for these two mixtures, the average aspect ratios, using either type of calculation, appear to be similar, i.e. to be independent of the polymer matrices employed. Quantitative information on aspect ratio distributions for such particles has only recently become a topic in the nanocomposite literature, so there is not much background against which to evaluate the significance of the differences between the two measures of average aspect ratio. It is straightforward, however; to determine if the variation in aspect ratio, in terms of the Halpin–Tsai theory of composites, would lead to a measurable change in modulus. Aspect ratios ranging from either 20–25 or 28–32 (the measured values given in Table 4) result in a calculated 2–4% change in the composite modulus, and this is not a difference that can be measured with a high level of confidence. Consequently, the measured aspect ratio averages shown in Table 4 may be substantially the same and independent of the polymer matrix employed.

In summary, the SAN/MMT nanocomposites have very nearly the same WAXS peak locations for each organoclay

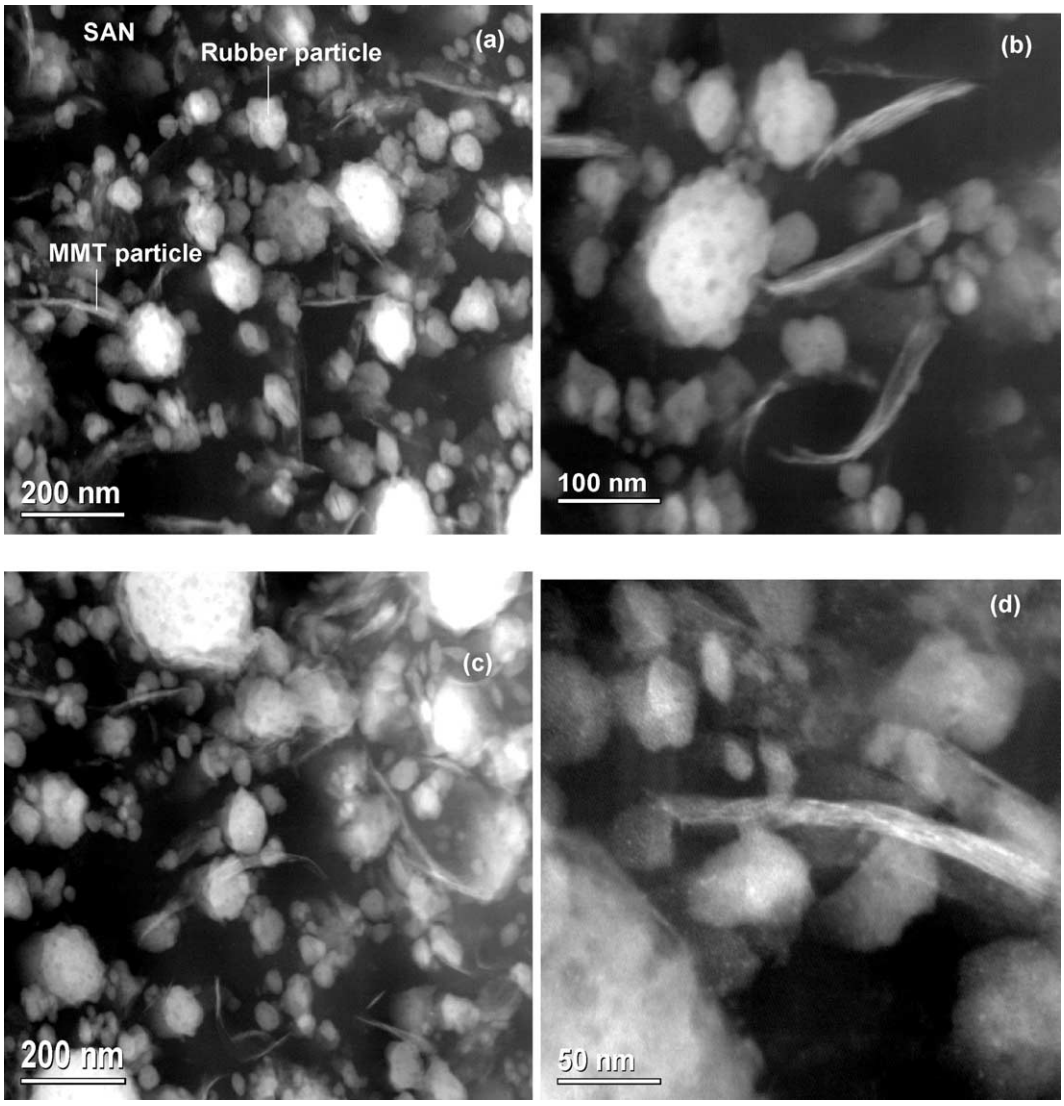


Fig. 6. STEM photomicrographs of ABS/$(HE)_2$MT composite at 3.0% MMT, stained. Both rubber particles and clay stacks appear bright, and SAN matrix is grey.

as those seen in ABS. TEM image analysis shows that the clay particles are about the same size in either matrix with the same aspect ratio averages, but that the efficiency of orientation does not appear to be as great for the ABS/MMT composites because of the interference of the rubber particles.

## 4. Mechanical property comparison

### *4.1. Young's modulus*

Representative stress/strain curves for ABS/MMT nanocomposites are shown in Fig. 8(a). These specimens yielded, but the elongation at break is reduced by addition of organoclay. Among the nanocomposites shown, the yield strengths are about the same, but for some clays increased MMT content resulted in a slight increase in yield strength. Representative stress-strain curves for SAN/MMT nanocomposites are shown in Fig. 8(b). SAN is a brittle material which breaks prior to yielding in tensile tests. Both the strength at break and the strain at break decrease with addition of organoclay.

Fig. 9 compares the response of the modulus of SAN and ABS on addition of the various organoclays plotted versus the MMT content in the nanocomposite. Notice that the modulus for virgin ABS is much lower than that of SAN, so that the scales for the two figures are different. In general, however, the reinforcement effect of the various organoclays followed the same order in either matrix. Quantitatively comparing the reinforcement effect in the two matrices, however, requires some method of accounting for the different matrix modulus and the different potential for reinforcement of each matrix.

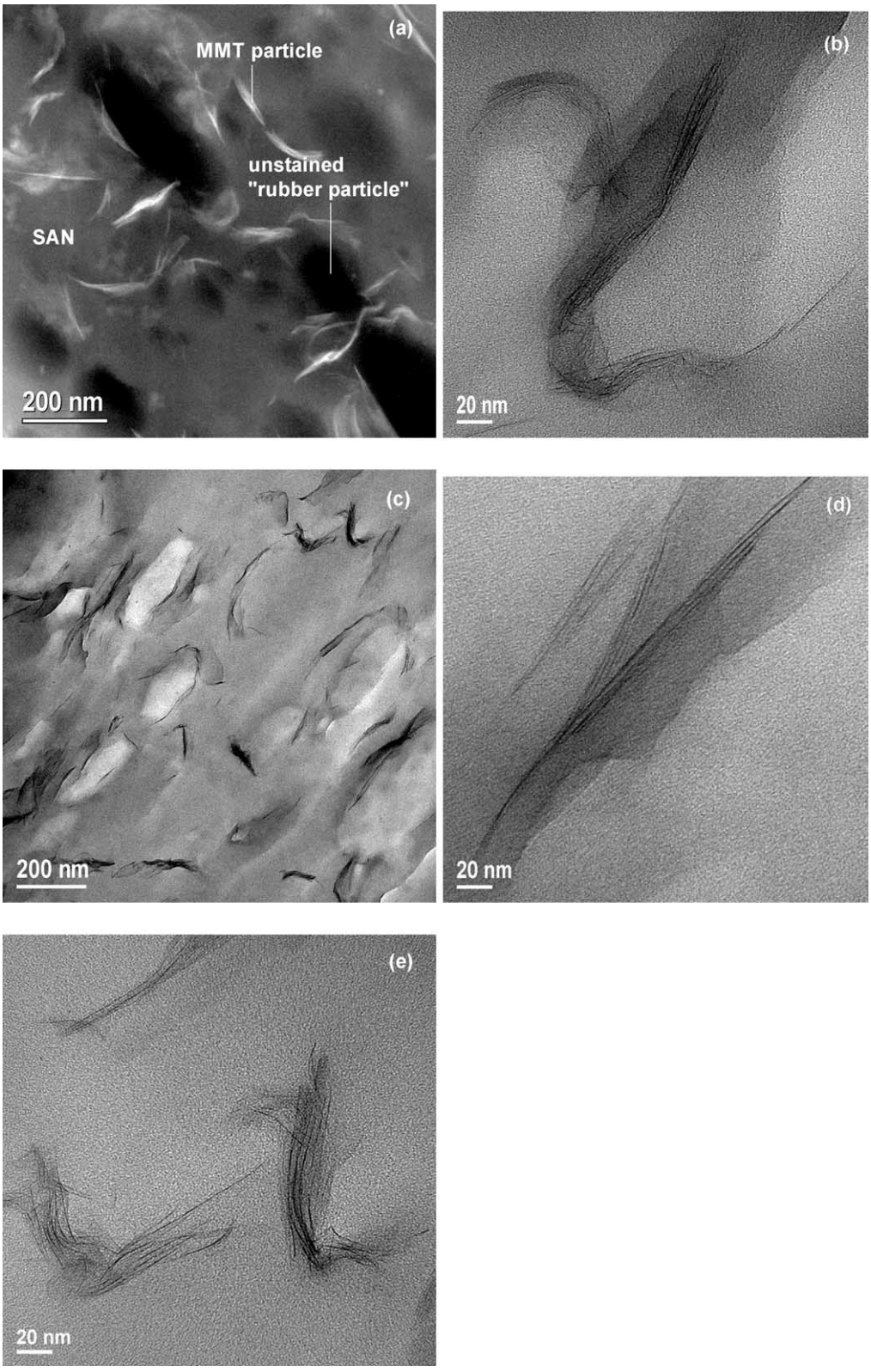


Fig. 7. STEM and TEM photomicrographs of ABS/$(HE)_2$MT composite at 3.0% MMT, unstained. Note presence of clay stacks oriented around rubber particles, which appear as holes in the matrix in this image.

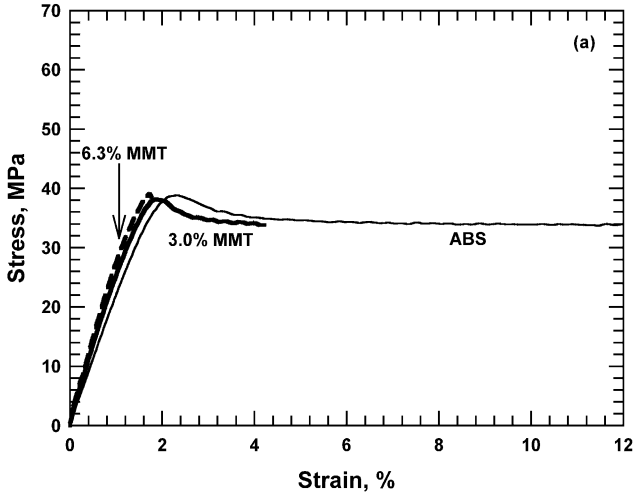


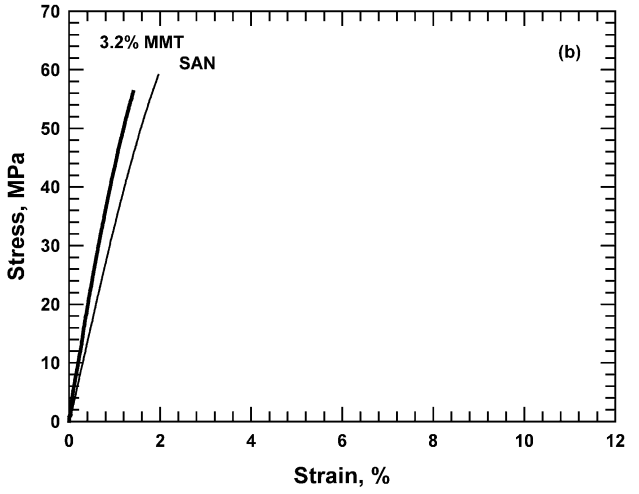


Fig. 8. Comparison of typical stress/strain diagrams for composites of (a) ABS/$M_2(HT)_2$ and (b) SAN/$M_2(HT)_2$.

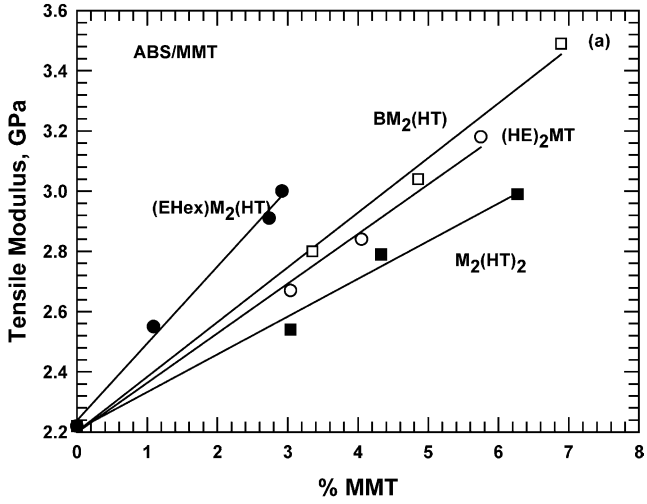


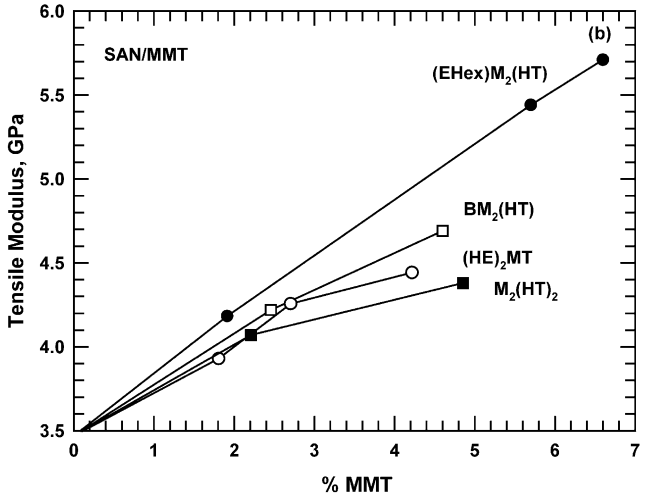


Fig. 9. Young's modulus versus MMT loading for composites of (a) ABS/MMT and (b) SAN/MMT.

### *4.2. Calculation of the reinforcement factor ($RF_w$) and exfoliation efficiency index (EEI)*

The reinforcement effect caused by montmorillonite clay particles for injection-molded nanocomposites is now generally understood to result substantially from the vast difference between the modulus of the matrix and the filler (the modulus of SAN is 3.47 GPa while that for MMT is 178 GPa), plus the combined contributions from a high aspect ratio and good orientation for well-exfoliated platelets [31,33]. Traditional composite theory offers a number of useful models for predicting the reinforcement effect; the models vary mainly in how the geometry of anisotropic particles are mathematically described and in the types of mathematical simplifications used. We have chosen to use the Halpin–Tsai theory because of the simplicity of the closed-form equation. There are differences in the prediction from the several other models available; however, these differences are relatively minor given the uncertainties encountered when defining the morphology of the clay particles.

Note that composite models assume that the composite consists of two phases, matrix and filler. However, three phases exist in ABS/MMT nanocomposites, namely the matrix, filler and rubber particles. In order to apply composite theory, we must make certain approximations for one pair of phases, e.g. we will approximate that the behavior of the matrix/rubber mixture can be represented with a single set of intrinsic properties. Alternatively, we could have instead assumed that the matrix/filler acts as a single phase. While comparing the two approaches just described is beyond the scope of the current study, Lee and Paul have explored this concept in greater detail as applied to polypropylene/elastomer/MMT nanocomposite behavior [34].

In this study, we use the modulus of the final

nanocomposite as an indication of the degree of dispersion of the filler. The pristine organoclay particles consist of nanometer-thin platelets aggregated into tactoids whose diameters are measured in microns. These tactoids provide limited reinforcement to the composite, because their aspect ratio is close to unity. As the aggregates are broken up and individual platelets peel away, the reinforcing phase can now have aspect ratios on the order of 100 or more. This increase in aspect ratio as the platelets exfoliate can be tracked by following the increasing composite modulus for a given volume fraction of filler.

Comparing the efficiency of modulus enhancement for nanocomposites requires one to identify a limit that the composite modulus could reach in the event of excellent exfoliation, and this limit depends on the magnitude of the matrix modulus. This is illustrated in Fig. 10 by predictions from the Halpin–Tsai theory for matrix moduli ranging from 0.1 GPa (e.g. polyethylene) up to 4.0 GPa (e.g. styrenic copolymers). For aspect ratios in the range of 20, the differences in reinforcement potential for a composite based on SAN ($E_m = 3.47$ GPa) versus a composite based on ABS ($E_m = 2.27$ GPa) is not substantial; however, at aspect ratios closer to 100, the difference is much more pronounced. Thus, some allowances for this may be necessary when comparing the reinforcing effect of clay in matrices of widely different moduli. One can approach the comparison of SAN and ABS reinforcement from at least two points of view. First, we might normalize the composite modulus by the matrix modulus, hereafter referred to as the reinforcement factor, $RF_w$. This approach assumes that the difference in reinforcement potential is small if the aspect ratios of the particles in the two composites being compared are not large. More rigorously, we could use composite theory to predict the limit for reinforcement (i.e. the modulus of a well-exfoliated system) in each matrix and subsequently calculate a reinforcement efficiency, hereafter referred to as the exfoliation efficiency index, EEI.

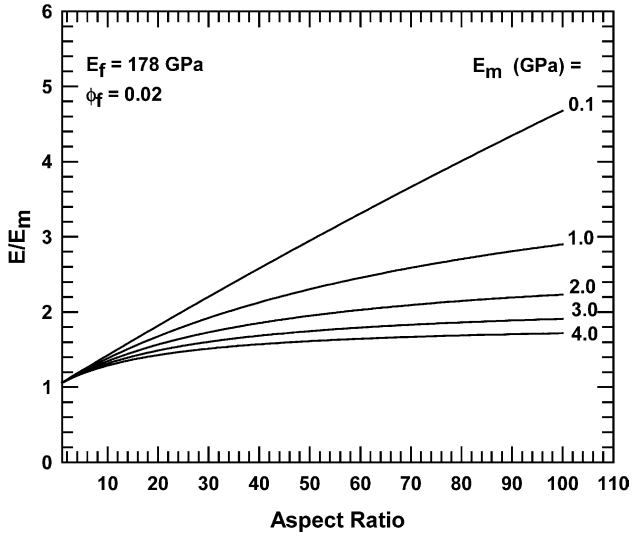


Fig. 10. Halpin–Tsai predictions of the normalized composite modulus, $E/E_m$, versus filler aspect ratio for composites of polymer and montmorillonite where the matrix modulus, $E_m$, varies from 0.1 for polyethylene to 4.0 for styrenic copolymers.

Calculation of a reinforcement factor, $RF_w$, has been discussed in previous publications [23], and is simply the slope of a loading curve for modulus taken at very low filler loadings,

$$RF_w = \lim_{\Delta w_f \to 0} \frac{d\left[\frac{E}{E_m}\right]}{dw_f} \tag{5}$$

In this case, for practical purposes, the weight fraction of filler, $w_f$, is used instead of volume fraction, $\phi_f$, where $E$ and $E_m$ are the moduli of the composite and the matrix, respectively.

Calculation of an exfoliation efficiency index, EEI, was suggested earlier by Fornes and Paul [35]. The value of the theoretical modulus for a well-exfoliated composite, referring back to Fig. 10, will depend on the matrix modulus and requires input of an aspect ratio representative of a fully exfoliated material. To illustrate, one might take the ultimate aspect ratio for very well-exfoliated platelets to be 100, as observed for nylon 6/MMT nanocomposites [31]. There is still some uncertainty about whether this value reflects the intrinsic size of the current organoclays or whether it depends on the process or matrix used to achieve exfoliation. Given an assumed limiting aspect ratio of 100; however, one can calculate a theoretical modulus from the Halpin–Tsai theory,

$$\frac{E}{E_m} = \frac{1 + \zeta\eta\phi_f}{1 - \eta\phi_f} \tag{6}$$

corresponding to a given volume or weight percent of MMT, where $E_m$ and $E$ are the moduli of the matrix and composite, respectively, $\phi_f$ is the volume fraction of the filler, and $\zeta = 2\times$(length/thickness) is the shape factor. The factor $\eta$ is calculated from the moduli of filler and matrix, and also involves the shape factor,

$$\eta = \frac{(E_f/E_m) - 1}{(E_f/E_m) + \zeta} \tag{7}$$

Calculation of the efficiency of exfoliation is then straightforward for a given volume percent of filler,

$$\text{exfoliation efficiency index} = \text{EEI} = \frac{E_{expt}}{E_{theory}} \tag{8}$$

### 4.3. Comparison of reinforcement effect in SAN/MMT versus ABS/MMT

Fig. 11 shows the reinforcement factors, or $RF_w$, for SAN composites versus ABS composites as a function of the shift in the gallery height ($\Delta d_{001}$). Overall, the $RF_w$ pattern for both matrices is qualitatively the same.

Values for the exfoliation efficiency indices, EEI, are shown in Fig. 12 for both SAN and ABS nanocomposites.

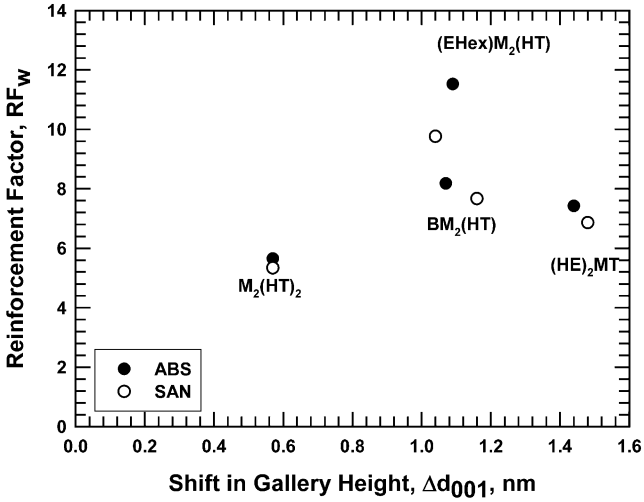


Fig. 11. Comparison of experimental reinforcement factors ($RF_w$) versus shift in gallery height ($\Delta d_{001}$) for ABS/MMT and SAN/MMT composites.

Assuming a well-exfoliated mixture would result in an aspect ratio of 100 for the filler, that the filler occupies 2 vol%, and has a modulus of 178 GPa, analogous to that of muscovite, [36,37] and density of 2.83 g/cm$^3$ as calculated from unit cell parameters and a surface area of 0.515× 8.9 nm$^2$ [38]. This comparison indicates that efficiency is consistently lower in the ABS matrix, which correlates well with the observation that the orientation of the clay particles is less perfect because they seem to conform to the rubber particle surfaces. Nevertheless, the same pattern is exhibited for a given clay, i.e. organoclays which are inefficient at producing modulus in SAN are also inefficient at producing modulus in ABS, and organoclays which are efficient at building modulus are similar for both matrices. Therefore, in terms of modulus enhancement, SAN is a good choice for modeling the clay/matrix interactions compared to the more complex ABS/MMT system.

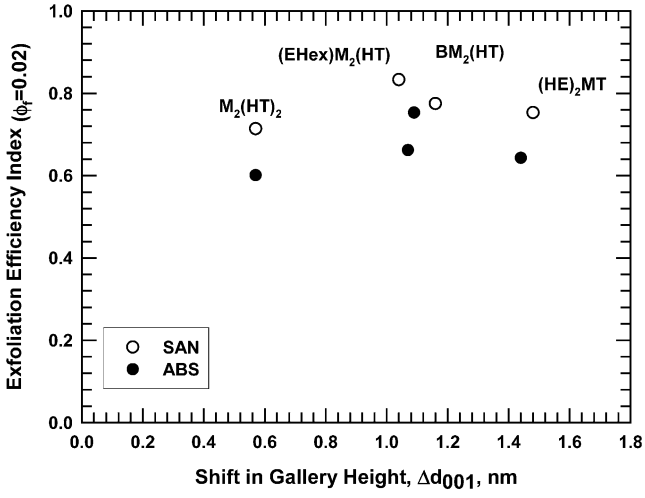


Fig. 12. Comparison of exfoliation efficiency index versus shift in gallery height ($\Delta d_{001}$) for ABS/MMT and SAN/MMT composites. These indices were calculated based on an assumed limiting aspect ratio of 100, and a filler volume fraction = 0.02. Note similar patterns of reinforcement for various organoclays in the two matrices.

### 4.4. Tensile strength

Fig. 13 shows the yield strengths of ABS/MMT composites and tensile strengths of SAN/MMT composites. In general, for ABS/MMT we see improvement in the yield strength as clay loading increases, depending on the choice of the organoclay. ABS/MMT composites which show the greatest increase in modulus also showed the greatest strength enhancement.

The SAN/MMT composites all fractured prior to yielding, since SAN itself is brittle; the tensile strengths reported were characterized by high standard deviations. Addition of clay for these materials resulted in a reduction in tensile strength, which was discussed in greater detail in a previous publication [23].

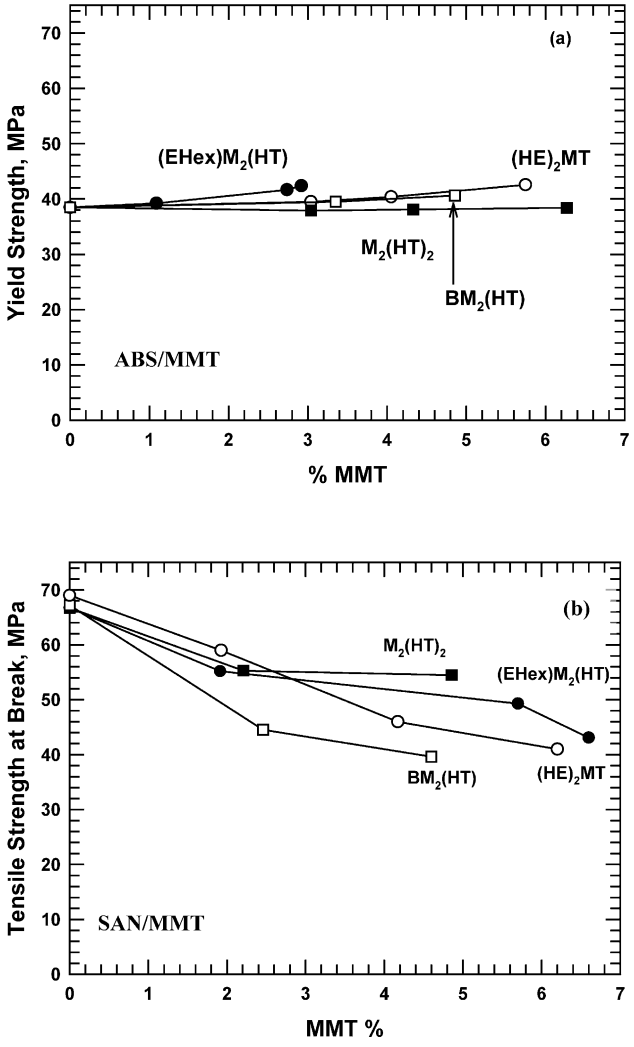


Fig. 13. Comparison of (a) tensile strength at yield behavior for composites of ABS/MMT and (b) tensile strength at break behavior for composites SAN/MMT.

### 4.5. Elongation and notched Izod impact

Elongation at break values are shown in Fig. 14 for the different organoclays used to form ABS/MMT composites. Here, the best retention of elongation was seen for the sample which showed the least reinforcement in modulus. Indeed, if a certain amount of organoclay was added, even the normally ductile ABS in some cases broke in a brittle fashion before yield. For traditional composites, addition of a reinforcing agent to a polymer generally decreases ductility. Nanophase reinforcing agents seem to result in a similar response based on observations to date.

Experimentally, the impact strength of nanocomposites of polymer/MMT are generally reported to decrease modestly, even for the highest levels of exfoliation [14,15,39]. The notched Izod test results for the ABS/MMT composites are shown in Fig. 15. Composites formed from all of the organoclays lead to reduced Izod impact strengths with no clear differentiation among the various organoclays. Materials used in electronic housings are expected to have approximately 200 J/m notched Izod; however, none of the samples in this initial study using a simple drop-in formulation maintained such a toughness value. In these materials, the rubber content, rubber morphology, and acrylonitrile content were all fixed, but varying these parameters in future studies might provide a better balance of mechanical properties for this application. In computer housings, recall that the MMT is added not for modulus improvement but for fire retardancy, and modulus improvement is not expected to be as critical in the balance of properties as toughness. Therefore, one approach for optimization of the formulation might be to increase the rubber content, which would improve toughness values, but simultaneously lower the composite modulus, and increase peak heat release rate and smoke production. Another approach is to optimize the acrylonitrile content, and the effects of acrylonitrile content on toughness have been

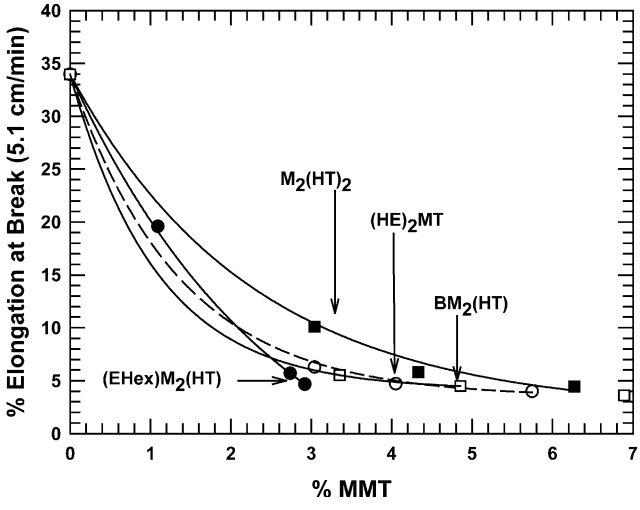


Fig. 14. % Elongation at break for composites of ABS/MMT.

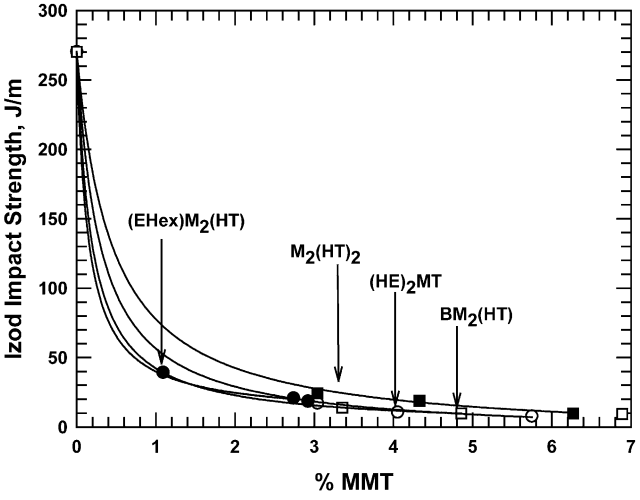


Fig. 15. Notched Izod impact strength trends for composites of ABS/MMT.

extensively described by Kim et al. [40,41]. A third approach is optimization of the rubber particle size. The rubber particles in the emulsion-made ABS used here are not large enough to be most effective for toughening. Use of other types of ABS materials with larger, more optimum-sized rubber particles might lead to a drop-in, nano-reinforced, nano-fire retarded ABS formulation that meets the impact specification.

## 5. Conclusions

These studies indicate that SAN/MMT nanocomposites effectively model the organoclay dispersion seen in more complex ABS/MMT nanocomposites. SAN is the matrix phase of the multiphase ABS system. TEM and STEM evidence are presented which show that the clay particles in a drop-in melt-processed ABS formulation reside in the SAN matrix phase, with some accumulation of MMT particles at the rubber surface which seem to conform to the rubber particle shape. No MMT particles were found in the ABS rubber phase which is not surprising. WAXS measurements for four different organoclays in the two matrices showed the same peak height and shift in gallery height ($\Delta d_{001}$) for each organoclay.

Comparing the reinforcement effect in SAN to that in ABS is complicated by the fact that the matrices have different moduli. Nevertheless, quantitative evaluation of the efficiency of modulus enhancement suggests that the patterns of exfoliation were the same, i.e. organoclays which are more efficiently exfoliated in SAN are also more efficiently exfoliated in ABS. The level of reinforcement in ABS was somewhat lower than in SAN, which is consistent with TEM evidence of accumulation of MMT particles at the rubber particle surfaces, resulting in less effective clay particle orientation. In general, it is concluded that in terms of compatibility, SAN/MMT composites are a good model

system for studying the more complex ABS/MMT composites.

## Acknowledgements

The authors would like to thank Dr Barbara Karn of the US Environmental Protection Agency and the Air Force Office of Sponsored Research for funding. We gratefully acknowledge interactions with the staff of Southern Clay Products, who provided materials and advice, including the WAXS performed by Randy Chapman. Dr Mario Miki Yoshida at the Center for Nano and Molecular Science and the Texas Materials Institute, University of Texas at Austin provided electron microscopy support. Thanks to Dow Chemical for the SAN and the General Electric for the ABS. Further, thanks to the Institute for Environmental and Industrial Science at Texas State University for logistics and funding.

## References

[1] Directive 2002/95/EC of the European Parliament and of the Council of 27 Jan 2003 on the restriction of use of certain hazardous substances in electrical and electronic equipment. OJ L 37/19 1323003; 2003.
[2] Hileman B. Chem Eng News 2002;80(26):15.
[3] Pescovitz D. Sci Am 2000;282(2):33.
[4] De Poortere M, Schonbach C, Simonson M. Fire Mater 2000;24:53.
[5] Simonson M, Stripple H. Eigth international conference of interflamm, Edinburgh, Scotland. London: Interscience Communications; 1999. p. 885.
[6] Simonson M. Polym Mater Sci Eng (Am Chem Soc) 2000;83:90.
[7] Weil ED. BCC conference flame retardancy, Stamford, CN. Norwalk, CN: Business Communications Co, Inc; 2001. p. 12.
[8] Bergman D. IPC white paper on halogen-free materials used for printed circuit boards and assemblies. USA: IPC Halogen-Free Materials Task Group; 2001.
[9] Bourbigot S, Devaux E, Flambard X. Polym Deg Stab 2002;75:397.
[10] Kashiwagi T, Harris Jr RH, Zhang X, Briber RM, Cipriano BH, Raghavan SR, et al. Polymer 2004;45:881.
[11] Gilman JW, Jackson CL, Morgan AB, Harris JD, Manias E, Giannelis EP, et al. Chem Mater 2000;12:1866.
[12] Wilke CA, Tidjani A. Polym Deg Stab 2001;74:33.
[13] Camino G, Zanetti M, Canavese D, Morgan AB, Lamelas FJ, Wilkie CA. Chem Mater 2002;14:189.
[14] Fornes TD, Yoon PJ, Keskkula H, Paul DR. Polymer 2001;42:9929.
[15] Mulhaupt R, Rerichert P, Nitx H, Klinke S, Raniner B, Thomann R. Macromol Mater Eng 2000;275:8.
[16] Hu Y, Wang S, Song L, Jie L, Chen Z, Fan W. J Appl Polym Sci 2004; 91(3):1457.
[17] Hu Y, Wang S, Song L, Wang Z, Chen Z, Fan W. Polym Deg Stab 2002;77:423.
[18] Zhang B, Song M, Hao G, Guo T. J Appl Polym Sci 2004;94:238.
[19] Wilkie CA, Zheng X. Polym Deg Stab 2003;82:441.
[20] Wilkie CA, Jiang DD, Su S. Polym Deg Stab 2004;83:333.
[21] Lee DC, Kang CM, Jang LW. J Polym Sci, Part B: Polym Phys 2001; 39:719.
[22] Hu Y, Wang S, Zong R, Tang Y, Chen Z, Fan W. Appl Clay Sci 2004; 25:49.
[23] Stretz HA, Paul DR, Keskkula H, Li R, Cassidy PE. Polymer, 2005;46:2621.
[24] Cho JW, Paul DR, Dennis HR, Hunter DL, Chang D, Kim S, White JL. Polymer 2001;42:9513.
[25] Cho JW, Paul DR. Polymer 2001;42:1083.
[26] Suter UW, Osman MA, Ploetze M. J Mater Chem 2003;13:2359.
[27] Fornes TD, Yoon JT, Keskkula H, Paul DR. Polymer 2002;43:2121.
[28] Williams DB, Carter CB. Imaging in the TEM. New York: Kluwer; 1996.
[29] Cheng TW, Paul DR, Keskkula H. Polymer 1992;33(8):1606.
[30] Bousmina M, Utracki LA, Suprakas SR, Pouliot S. Polymer 2004;45: 8403.
[31] Fornes TD, Paul DR. Polymer 2003;44:4993.
[32] Chavarria F, Paul DR. Polymer 2004;45:8501.
[33] Sheng N, Boyce MC, Parks DM, Rutledge GC, Abes JI, Cohen RE. Polymer 2004;45:487.
[34] Lee HS, Fasulo PD, Rodgers WR, Paul DR. In preparation.
[35] Fornes TD, Paul DR. Macromolecules 2004;37:7698.
[36] Alexandrov KS, Ryshova TV. Bull Acad Sci USSR 1961;12:1165.
[37] McNeil LE, Grimsditch M. J Phys: Condens Matter 1993;5(11):1681.
[38] Van Olphen H. An introduction to clay colloid chemistry. New York: Wiley; 1977.
[39] Kojima Y, Usuki A, Kawasuma M, Okada A, Kurauchi T, Kamigaito O. J Polym Sci, Part A: Polym Chem 1993;31(4):983.
[40] Kim H, Keskkula H, Paul DR. Polymer 1991;32(8):1447.
[41] Kim H, Keskkula H, Paul DR. Polymer 1990;31(5):869.